Supporting Information

Trinuclear copper supramolecular framework for boosting electrocatalytic reduction of CO_2 to C_3 product

ShenXia Huang, [abe] Zhanfeng Ju, [b] Jing Lin, [bd] Wan Lin, *[bce] and Yaobing Wang *[abcde]

[a] College of Chemistry and Materials Science, Fujian Normal University, Fuzhou, 350007, China.

[b] CAS Key Laboratory of Design and Assembly of Functional Nanostructures, and Fujian Provincial Key Laboratory of Nanomaterials, State Key Laboratory of Structural Chemistry, Fujian Institute of Research on the Structure of Matter, Chinese Academy of Sciences, Fuzhou 350002, Fujian, P. R. China.

[c] University of Chinese Academy of Sciences, Beijing 100049, P. R. China.

[d] Fujian Science and Technology Innovation Laboratory for Optoelectronic Information of China, Fuzhou 350108, Fujian, P. R. China.

[e] Fujian College, University of Chinese Academy of Sciences, Fuzhou 350002, P. R. China.

[*] Corresponding Author: wangyb@fjirsm.ac.cn; linwan@fjirsm.ac.cn

Experimental Section

Materials

All chemicals and solvents are commercially available and can be used without further purification unless otherwise stated. Acetonitrile (CH_3CN), methanol (CH_3OH), ethanol (C_2H_5OH) and potassium bicarbonate ($KHCO_3$) were purchased from Sinopharm Chemical Reagent Co. Methyl 3,5-dialdehyde-4-hydroxybenzoate, cyclohexanediamine, and potassium chloride were purchased from McLean Biochemistry Co. Tetrahydrofuran, copper formate, phenol, chloroform, and deuterated water were purchased from Adamas. nafion membrane fluid was purchased from Shanghai Hesen Electric Co. The gaseous reagents, including carbon dioxide (99.999%) and argon (99.999%), were supplied by Xinhua Natural Gas Corporation (Fuzhou, China).

Materials characterizations

The synthesis of the validated materials was tested using AVANCE III HD ^1H NMR spectrometer from Bruker, Germany. PXRD characterization tests were performed on RIGAKU Miniflex600. Single crystal data was collected with a SuperNova single crystal diffractometer from Rigaku, Japan. X-ray photoelectron spectroscopy (XPS) was recorded with a Thermo Kalpha instrument. Scanning electron microscopy (SEM) field emission was performed with an SU8010 at 5 kV. Gas products were analyzed by gas chromatography (GC 9790plus FULI) and liquid products were detected by gas chromatography (GC 9720 FULI). Isotope labeling experiments were performed using $^{13}CO_2$ instead of $^{12}CO_2$, and liquid product ^1H NMR detection results were analyzed by ECZ400S spectrometer. Electrochemical tests were performed using CHI660E electrochemical workstation (Shanghai Chenhua Instrument Co., Ltd.).

Electrochemical Measurements

Preparation of cathode electrodes

The electrocatalyst preparation was initiated by pulverizing 5 mg of material into fine powder, followed by homogeneous dispersion in a solvent blend (300 μL H_2O:600 μL MeOH:100 μL Nafion) under ultrasonication to form a colloidally stable ink. Precise deposition of 100 μL ink via micropipette onto dual-sided carbon paper (0.5 cm^2 × 2) achieved 0.5 mg/cm^2 loading, with subsequent IR lamp drying for electrochemical characterization. Nafion (5 wt%) served as both polymeric binder and dispersant, ensuring uniform catalyst distribution across the carbon substrate during working electrode assembly.

Catalytic evaluation

The electrochemical evaluation of the CO_2 reduction reaction (CO_2RR) was performed at ambient temperature utilizing an electrochemical workstation (CHI-660E) within an H-type electrolytic cell, comprising a hermetically sealed dual-compartment reactor partitioned by a proton exchange membrane (Nafion NRE 211). The measurements were carried out in an aqueous 0.1 M $KHCO_3$ electrolyte solution (pH = 6.8). For the working electrode, hydrophobic carbon paper uniformly deposited with an electrocatalyst suspension was utilized in the electrochemical assessments. All potentials were measured relative to an Ag/AgCl reference electrode with 90% iR compensation, and results were reported relative to the reversible hydrogen electrode (RHE) according to the Nernst equation: E (V vs. RHE) = E (V vs. Ag/AgCl) + 0.197 + 0.059 × pH. The Faradaic efficiency (FE) of hydrocarbon formation was calculated as described.

The optimal potential window for catalytic evaluation was determined using linear sweep voltammetry (LSV), with the scan performed at a rate of 50 mV/s from 0 to -1.3 V (vs. RHE). The electrochemical surface area (ECSA) was quantitatively analyzed using the double-layer capacitance (CV) derived from cyclic voltammetry. All non-Faradaic CVs for ECSA determination were collected between 0.047 and 0.055 V vs. RHE at scan rates of 1-40 mV/s. Prior to CV characterization, the electrolyte was subjected to CO_2 saturation via continuous bubbling for a duration of 30 minutes.

Product analysis

The gaseous products (H_2, CO, CH_4, and C_2H_4) were characterized using a gas chromatograph (GC9720) equipped with dual detection systems: a flame ionization detector (FID) for monitoring hydrocarbon species (CO, CH_4, C_2H_4) and a thermal conductivity detector (TCD) for quantifying H_2. Ultra-high-purity argon (99.9995%) served as the carrier gas. Following a minimum reaction duration of 2 hours, the evolved gases were collected for compositional analysis. Concurrently, liquid-phase products from the cathode chamber were sampled during electrolysis. In nuclear magnetic resonance spectroscopy, an analytical mixture was formulated by combining 600 μL electrolyte, 70μL deuterium oxide, and 30μL of standard solution with 10 mM dimethyl sulfoxide concentrations. Quantitative assessment of CO_2 reduction reaction (CDRR) products was performed on a 400 MHz Inova NMR spectrometer employing a presaturation pulse sequence to suppress water signals.

Quantification of the faradaic efficiencies (FEs) was achieved through implementation of the subsequent mathematical expression:

$$FE(\%) = \frac{Q_{Product}}{Q_{Total}} \times 100\% = \frac{n_{Product} \times N \times F}{j \times t} \times 100\%$$

j = Partial current density of a specific product, A;

n = The number of electrons involved in the reduction products, which is 2 for CO and H_2; 2 for HCOOH; 8 for CH_4; 12 for C_2H_4; 12 for C_2H_5OH; and 18 for n-PrOH.F = Faraday's constant, 96485 C/mol;

N = mole fraction of product;

V = total molar flow rate of gas

Isotope labeling experiments were conducted using $^{13}CO_2$ under conditions nearly identical to those for $^{12}CO_2$.

Syntheses method

Synthesis of methyl 3,5-dialdehyde-4-hydroxybenzoate(L)

The synthesis procedure was initiated by introducing hexamethylenetetramine (25.38 g) and methyl p-hydroxybenzoate (6.8 g) into a 500 mL reaction vessel. Tetrahydrofuran (50 mL) was then introduced, and the mixture was subjected to 95°C heating with continuous stirring for 96 hours. After cooling, the addition of 350 mL deionized water and subsequent reflux treatment ensured complete dissolution, with yellow needle-shaped crystals forming upon gradual cooling to room temperature. After filtration, wash with water and dry in a vacuum oven for 1 day to give about 70% yield.

Synthesis of L^A

A quantity of 4.16 g of methyl 3,5-dialdehyde-4-hydroxybenzoate was dissolved in 80 mL of acetonitrile under continuous stirring in an ice bath. To this solution was added dropwise 30 mL of a methanolic solution containing 2.28 g of cyclohexanediamine, resulting in the immediate formation of a yellow precipitate. The reaction mixture was maintained under stirring at ice-bath temperature for an additional 12 hours, after which the solid product was isolated by filtration. The obtained yellow solid was subsequently purified by washing with minimal amounts of methanol, followed by vacuum desiccation, yielding 4.9 g of compound L^A (approximate yield: 85%). ^{1}H NMR (400 MHz, Chloroform-d δ): 14.97 (s, 3H), 8.65 (s, 3H), 8.42 (d, 3H), 8.24 (s, 3H), 7.87 (d, 3H), 3.81 (s, 9H), 3.54 (m, 3H), 3.32 (m, 3H), 1.76 (m, 24H). ^{13}C NMR (101 MHz, Chloroform-d δ): 168.43, 166.39, 163.90, 155.96, 136.45, 131.58, 124.61, 118.93, 117.71, 71.83, 51.97, 33.24, 33.07, 24.43, 24.23.

Synthesis of L^B

Charging a 250 mL round-bottomed flask with 4 g of L_A, 60 mL of THF, and 40 mL of methanol, the mixture was cooled in an ice bath before the gradual addition of 4 g $NaBH_4$, followed by 12-hour stirring under maintained cooling. After quenching with 6 mL of H2O and stirring for half an hour, the solvent was removed by rotary evaporation. After dilution with water (200 mL), the desired product was obtained as a white solid by filtration, washed with water and finally dried under vacuum. Through vacuum desiccation, product L^B was isolated with an approximate yield of 92%.^{1}H NMR (400 MHz, Chloroform-d δ): 7.66 (s, 6H), 3.79 (m, 21H), 2.57 (s, 6H), 1.98 (m,6H), 1.76 (m, 6H), 1.26 (m, 12H); ^{13}C NMR (151 MHz, Chloroform-d δ): 167.61, 130.62, 124.69, 115.42, 59.33, 51.53, 46.29, 30.71, 25.02.

Synthesis of Cu_3-HCOO

100 mg L^B and 100 mg $Cu(CH_3COO)_2{\cdot}H_2O$ in a 20 mL vial, add 6 mL of H_2O and 5 mL of ethanol. Heat it in a 65°C oven for two days, remove it, allow it to cool, and slowly evaporate to obtain dark green crystals. Wash them slightly with water, dry them, and the yield is approximately 65%.

Synthesis of Cu_3-SO_4

100 mg L^B and 100 mg $CuSO_4$ in a 20 mL vial, add 6 mL of H_2O and 5 mL of ethanol. Heat it in a 65°C oven for two days, remove it, allow it to cool, and slowly evaporate to obtain dark green crystals. Wash them slightly with water, dry them, and the yield is approximately 82%.

Synthesis of Cu_2-HCOO : 41.6 mg of L was dissolved in 2 mL of methanol. After cooling, 2 mL H_2O, 38 mg $Cu(CH_3COO)_2{\cdot}H_2O$, and 22.8 mg cyclohexanediamine were added. The vial was sealed and heated in a 65°C oven for 3 days, yielding dark green crystals with a yield of approximately 80%.

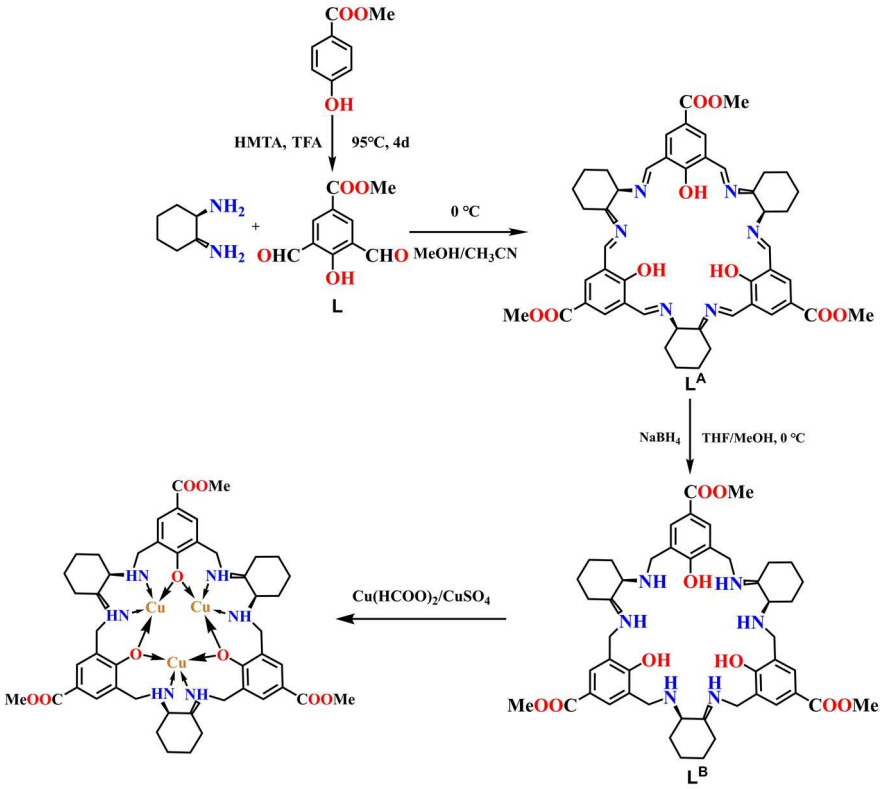

Scheme S1. Synthesis of Cu_3-HCOO and Cu_3-SO_4.

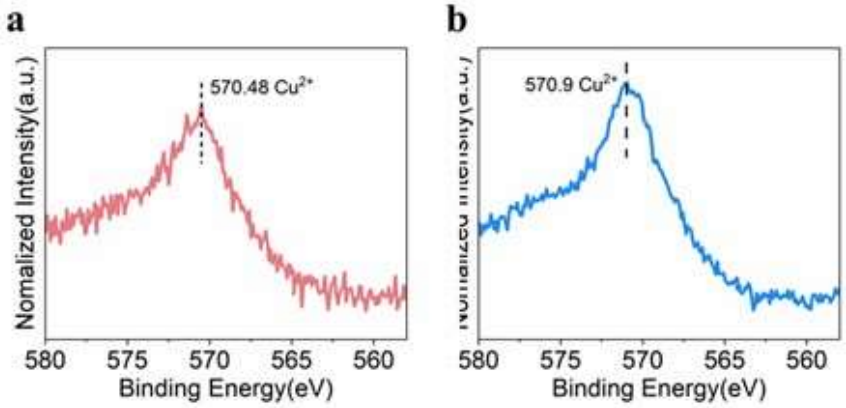

Figure S1. (a) Cu LMM spectra of Cu_3-HCOO. (b) Cu LMM spectra of Cu_3-SO_4.

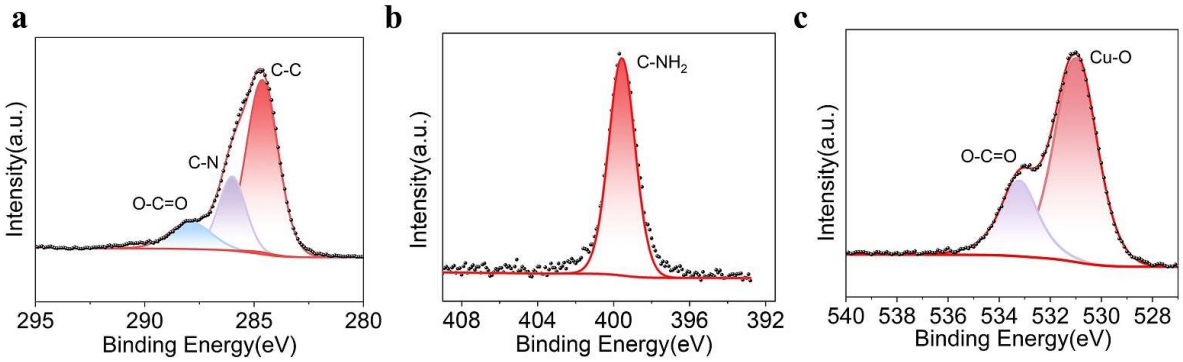

Figure S2. XPS spectra of Cu_3-HCOO (a) C 1s (b)N 1s (c)O 1s

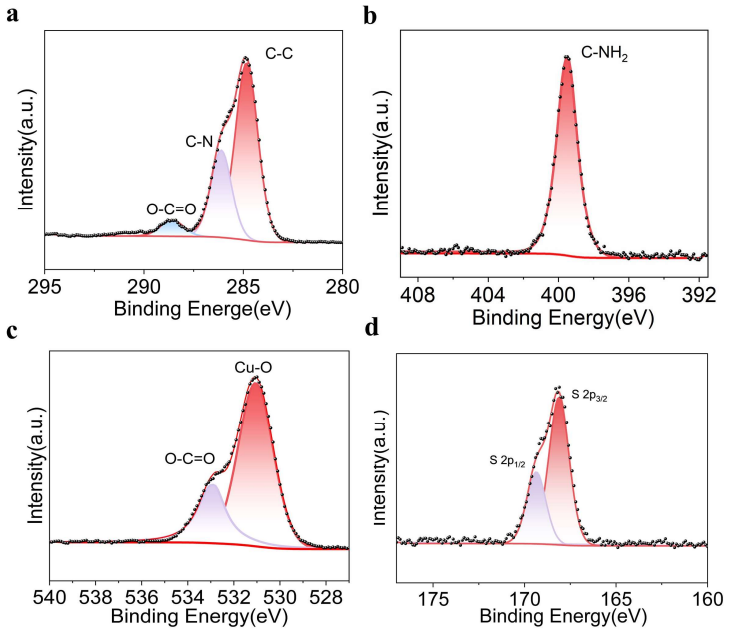

Figure S3. XPS spectra of Cu_3-SO_4 (a) C 1s. (b)N 1s. (c)O 1s. (d)S 2p

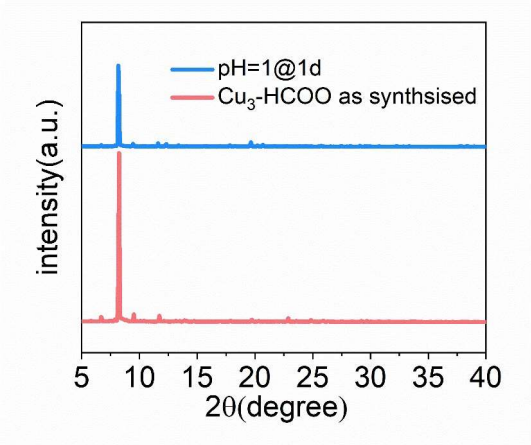

Figure S4. XRD patterns of experimental (red) and after soaking in HCl (pH=1) solution for 24 h (blue) of Cu_3-HCOO.

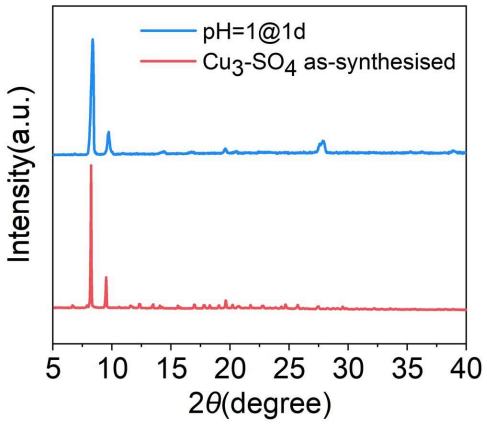

Figure S5. XRD patterns of experimental (red) and after soaking in HCl (pH=1) solution for 24 h (blue) of Cu_3-SO_4.

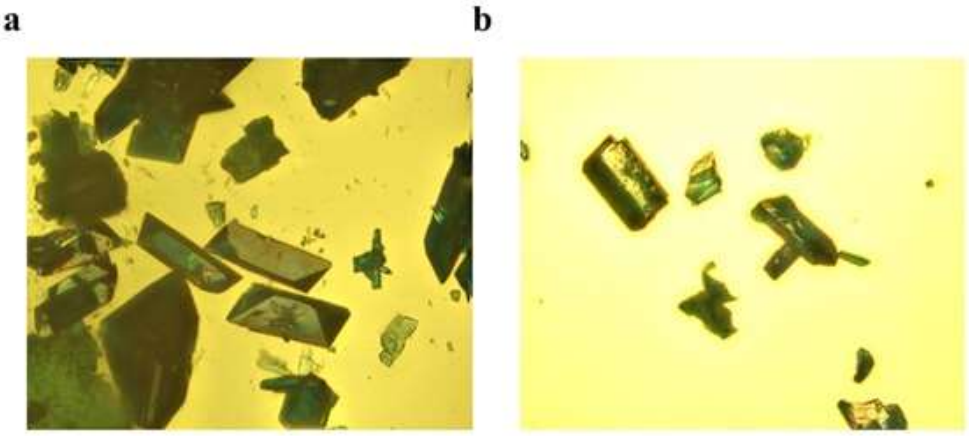

Figure S6. The optical microscope images of Cu_3-HCOO.

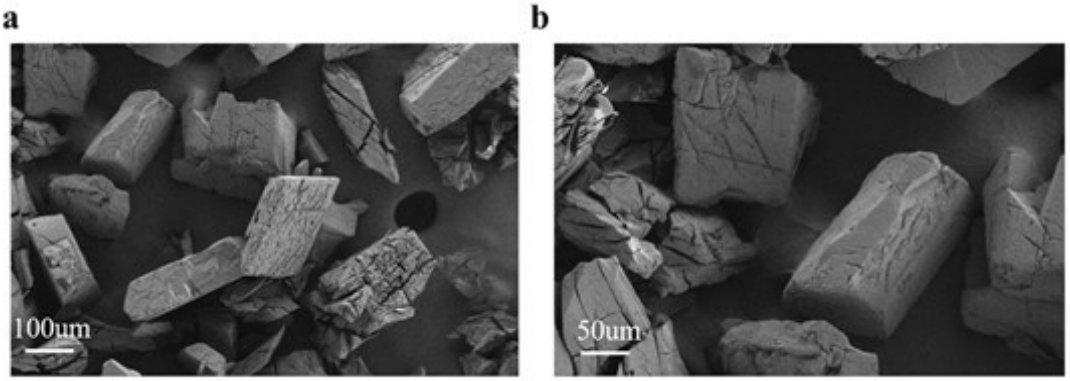

Figure S7. SEM images of Cu_3- SO_4.

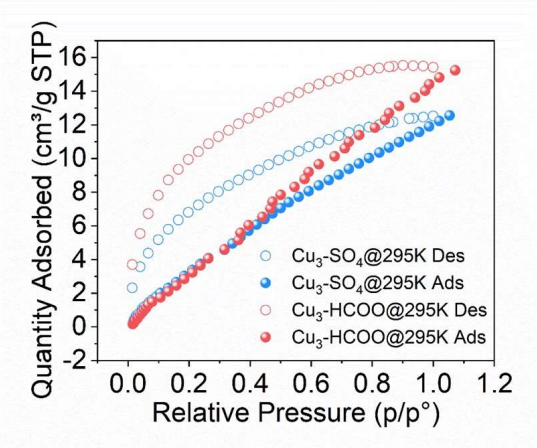

Figure S8. CO_2 adsorption and desorption spectra of Cu_3–HCOO and Cu_3–SO_4 at room temperature.

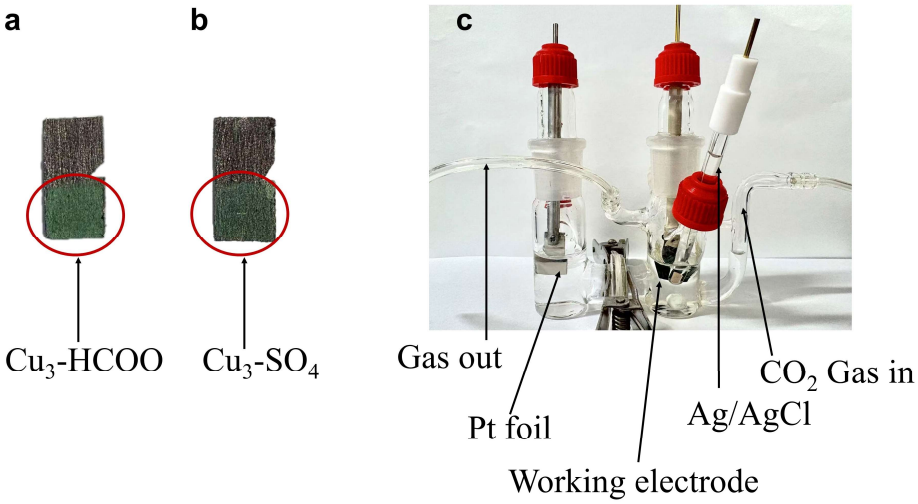

Figure S9. Photo of (a) Cu_3-HCOO electrode; (b) Cu_3-SO_4 electrode; (c) CO_2 electrochemical reduction cell.

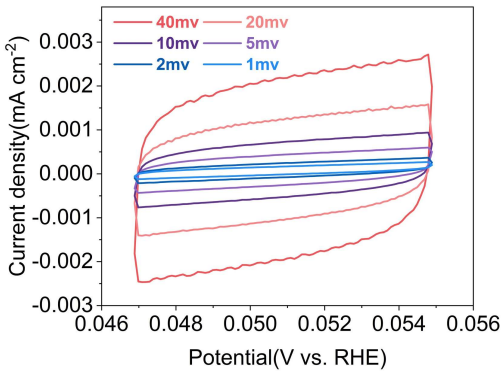

Figure S10. Cyclic voltammetry (CV) curves in the region of 0.047 ~0.055 V vs. RHE at various scan rate (1 ~ 40 $mV \cdot s^{-1}$) and corresponding capacitive current of Cu_3-HCOO.

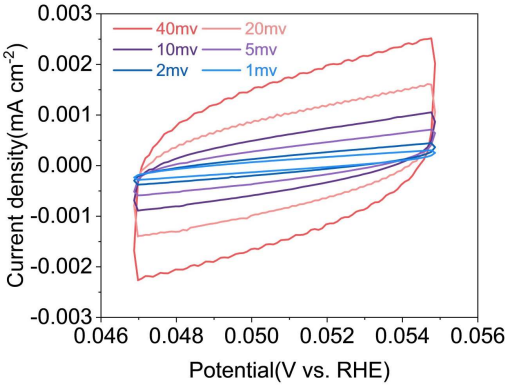

Figure S11. Cyclic voltammetry (CV) curves in the region of 0.047 ~0.055 V vs. RHE at various scan rate (1 ~ 40 $mV \cdot s^{-1}$) and corresponding capacitive current of Cu_3-SO_4.

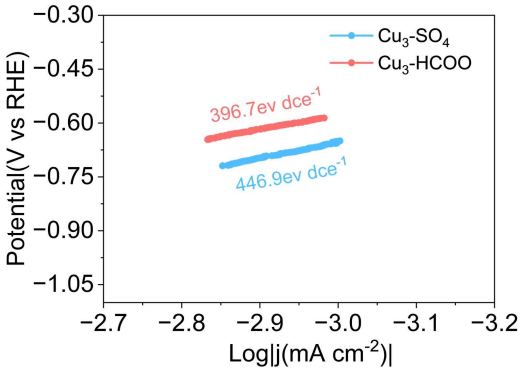

Figure S12. Tafel slope of Cu_3-HCOO and Cu_3-SO_4.

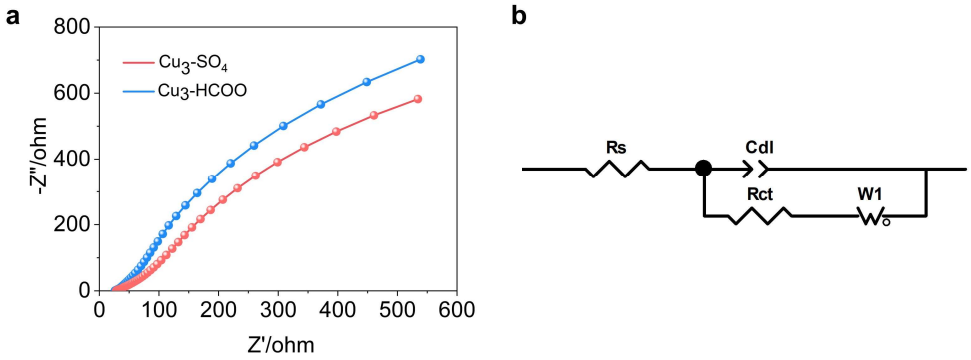

Figure S13. (a) EIS of Cu_3-HCOO and Cu_3-SO_4 (b) Equivalent circuit model simulated by Z-view.

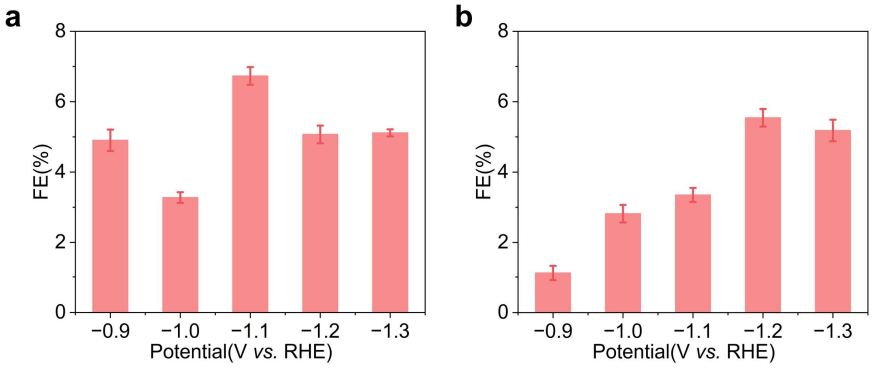

Figure S14. FE (n-PrOH) production by Cu_3-HCOO (a) and Cu_3-SO_4 (b) at various potentials.

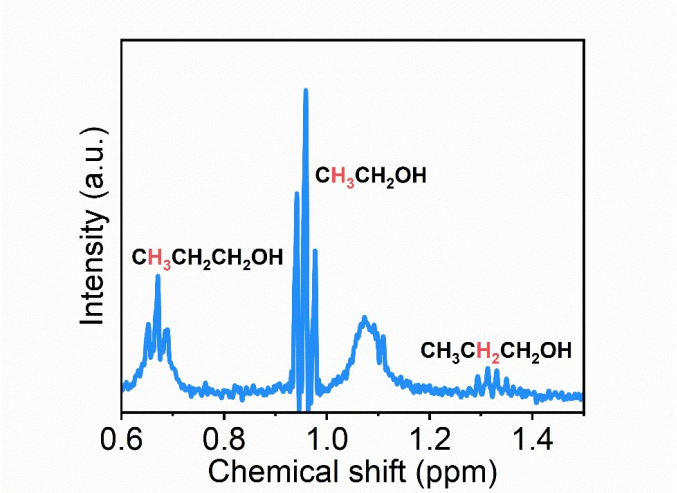

Figure S15. The ^{1}H NMR spectrum of Cu_3-HCOO liquid product in the range of 0.6-1.5 ppm.

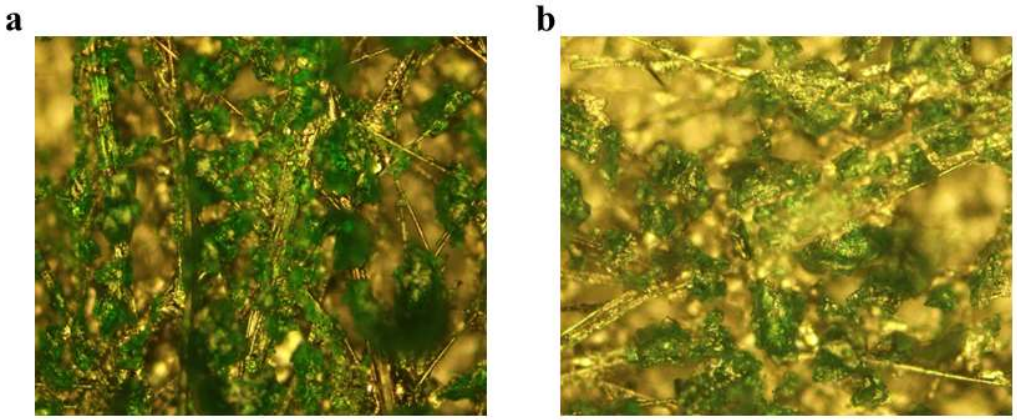

Figure S16. The optical microscope images of Cu_3-HCOO coated on carbon paper before (a) and after (b) catalysis.

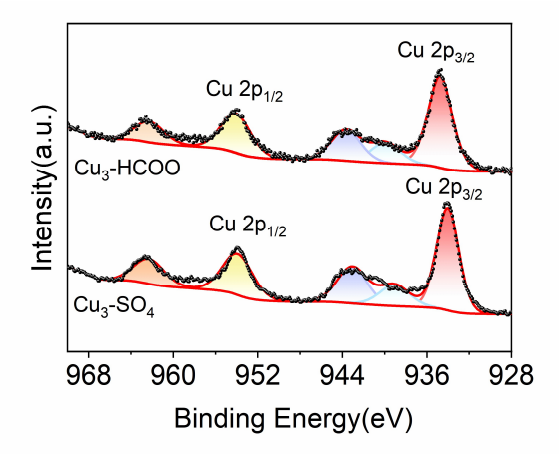

Figure S17. The XPS High-resolution Cu 2p spectra after electrochemical CDRR of Cu_3-HCOO and Cu_3-SO_4

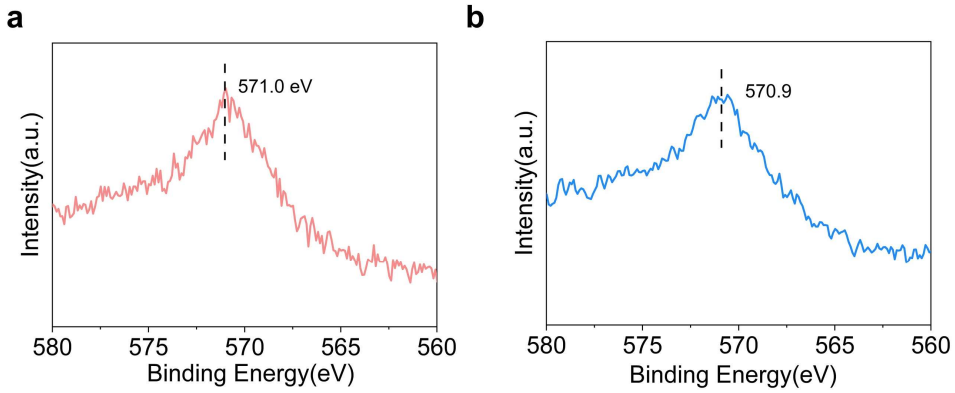

Figure S18. Cu LMM spectra after electrochemical CDRR. (a) Cu_3-HCOO (b) Cu_3-SO_4.

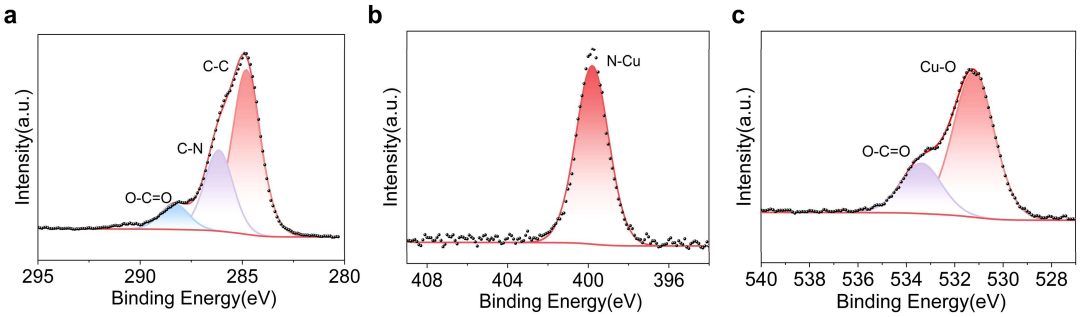

Figure S19. High-resolution XPS spectra of Cu_3-HCOO after electrochemical CDRR (a) C 1s. (b) N 1s. (c) O 1s.

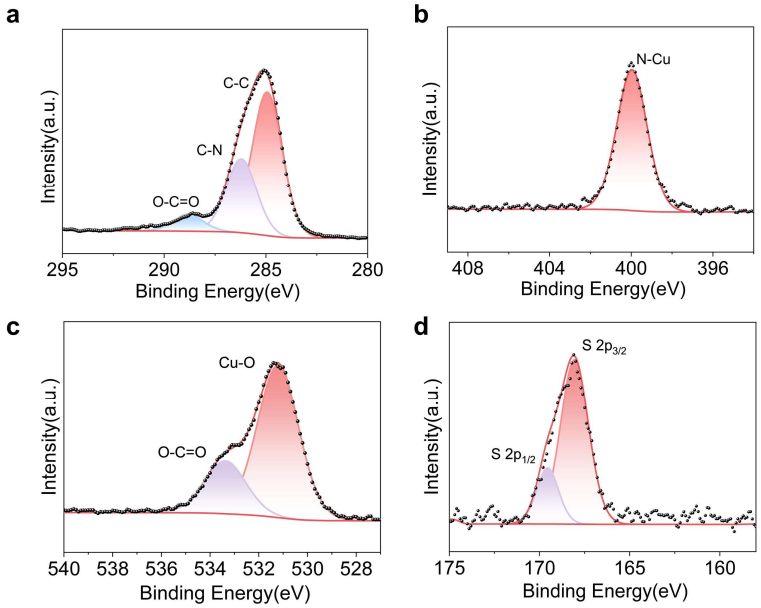

Figure S20. High-resolution XPS spectra of Cu_3-SO_4 after electrochemical CDRR (a) C 1s. (b) N 1s. (c) O 1s. (d) S 2p.

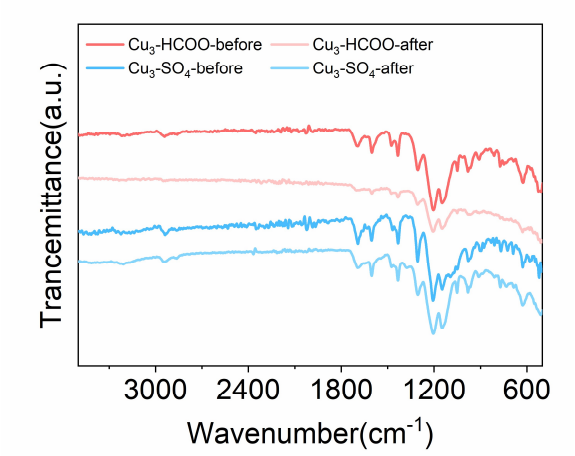

Figure S21. The FTIR spectra of before and after electrochemical CDRR of Cu_3-HCOO and Cu_3-SO_4

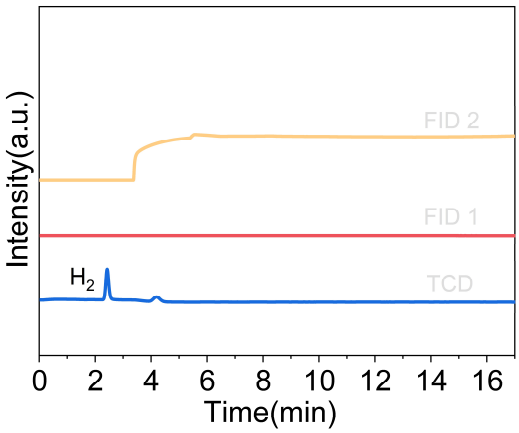

Figure S22. The gas chromatography (GC) spectrum of the electrolysis conducted using Cu_3-HCOO as the electrocatalyst under an Ar atmosphere.

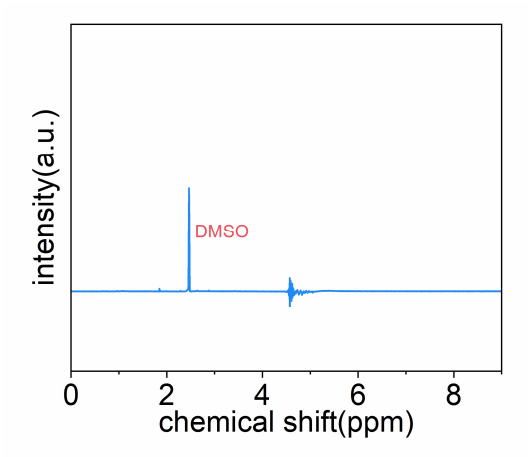

Figure S23. Cu_3-HCOO was immersed in the electrolyte without applying any potential, and combining 600μL electrolyte, 70μLD_2O, and 30μL of standard solution with 10 mM DMSO concentrations was taken for NMR testing.

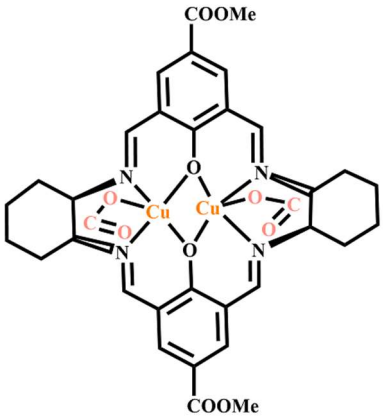

Figure S24. Molecular structure of Cu_2-HCOO.

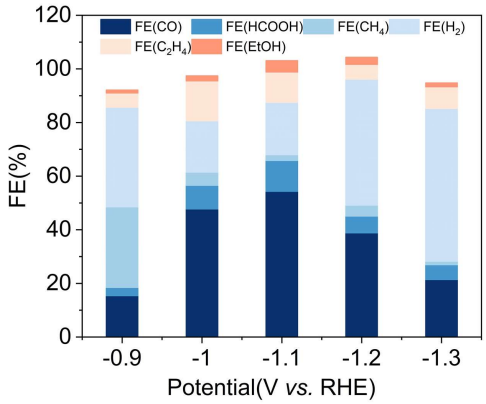

Figure S25. Faraday efficiency (FE) of different reduction products of Cu_2-HCOO.

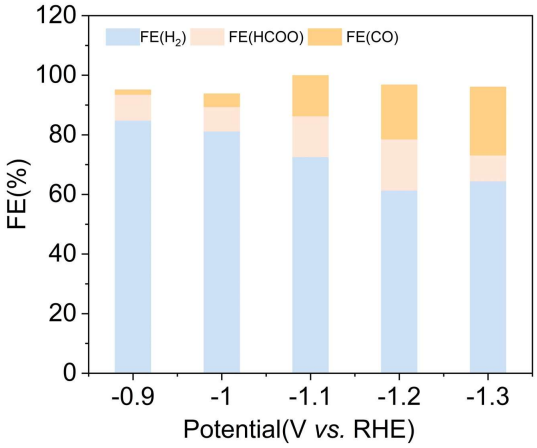

Figure S26. Faraday efficiency (FE) of different reduction products of Cu_3-HCOO in 0.1M $NaHCO_3$.

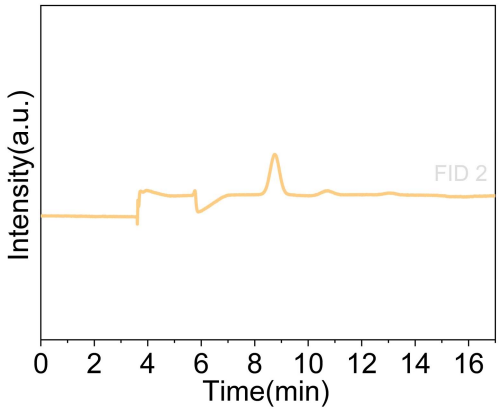

Figure S27. GC profiles of gas products of Cu_3-HCOO at -1.1 V vs. RHE.

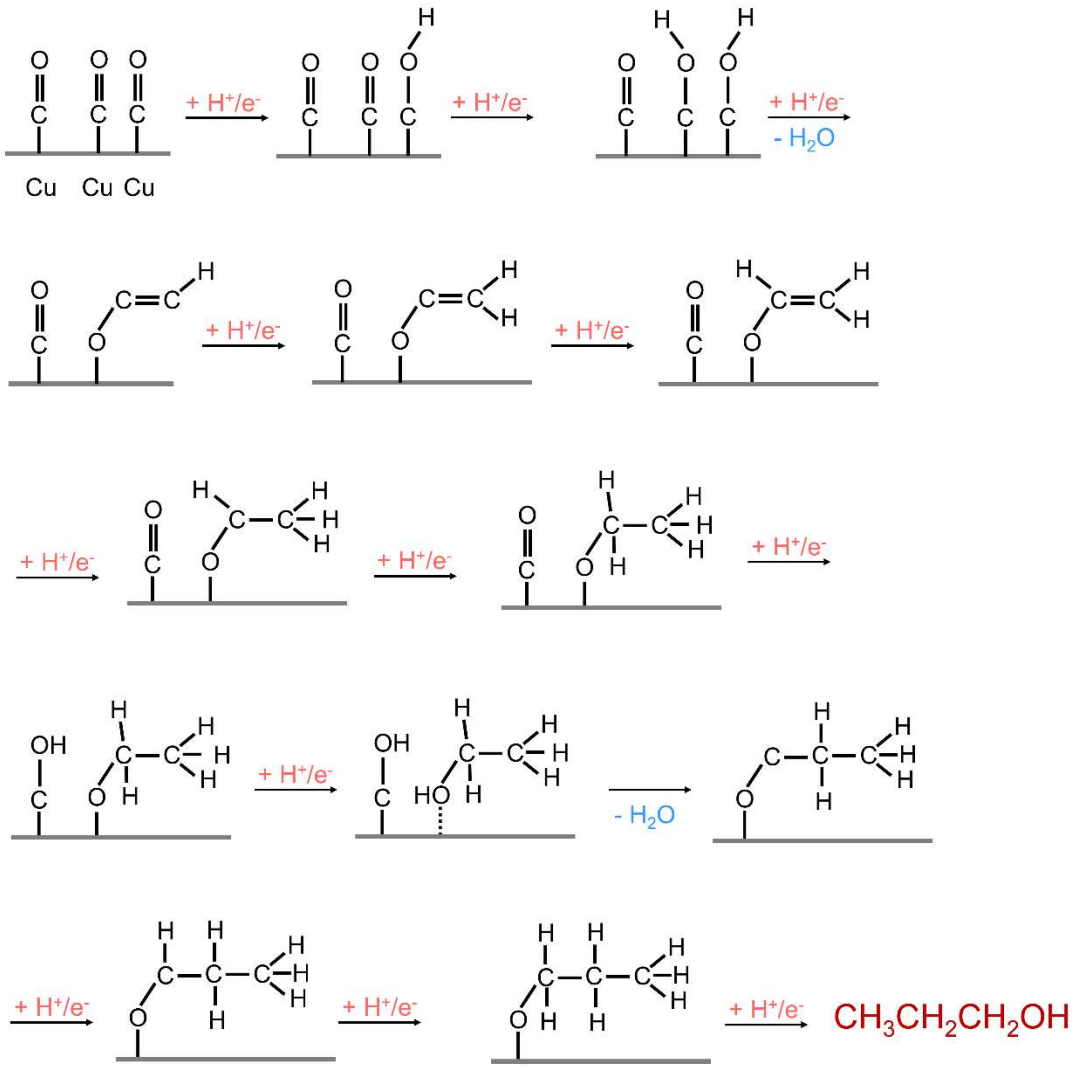

Figure S28. Schematic diagram of multi-step proton coupled electron transfer process for Cu_3-HCOO catalyzed reduction of CO_2 to propanol.

Table S1. Crystal data and structure refinement of Cu_3-SO_4 and Cu_3-HCOO.

	Cu_3-SO_4	Cu_3-HCOO
Empirical formula	CHCuNOS	CHNOCu
Formula weight	138.63	106.57
Crystal system	cubic	triclinic
Space group (number)	$F4_132$	$P-1$
a [Å]	37.30060(10)	12.51530(10)
b [Å]	37.30060(10)	16.0685(2)
c [Å]	37.30060(10)	16.7059(2)
α [°]	90	112.2900(10)
β [°]	90	95.8210(10)
γ [°]	90	100.9430(10)
Volume [Å^3]	51897.6(2)	2995.89(6)
Z	484	1
ρ_{calc} [gcm^{-3}]	2.147	0.059
μ [mm^{-1}]	10.266	0.202
F(000)	32428.0	51.0
Goodness-of-fit on F^2	5.576	2.046
Final *R* indexes [$I \geq 2\sigma(I)$]	R_1 = 0.2147 wR_2 = 0.5230	R_1 = 0.1059 wR_2 = 0.2806
Final *R* indexes [all data]	R_1 = 0.2248 wR_2 = 0.5447	R_1 = 0.1119 wR_2 = 0.2854
CCDC Number	2481124	2481123

Table S2 Comparison of the performances of catalysts on electrocatalytic CDRR to n-PrOH.

Catalyst	Electrolyte	E vs. RHE (V)	*j* (mA/cm^2)	FE% (n-propanol)	Ref.
Cu_3-HCOO	0.1M $KHCO_3$	-1.1	2.82	6.7	This work
Cu_3-SO_4	0.1M $KHCO_3$	-1.2	3.98	5.57	
Electrodeposited Cu nanocubes	0.1M $KHCO_3$	-1.05	0.28	1.3	5
MoS_2 thin film	0.1M KH_2PO_4	-0.59	0.26	3.5	6
Evaporated CuAu	0.1M $KHCO_3$	-0.97	0.39	4.72	7
N-substituted pyridinium modified Cu	0.1M $KHCO_3$	-1.1	1.1	11.8	8
Cu nanosphere	0.1M $KHCO_3$	-1.1	0.17	4.3	9
Commercial Cu powder	1M $KHCO_3$	-0.97	13.8	4.6	10
Au/Cu NR (NR2)	1 M KOH	-0.47	16.6	11.1	11
b-Cu_2O/Cu	0.1M $KHCO_3$	-1.4	6.8	16.2	12
Cu_2S-Cu-V	0.1M $KHCO_3$	-0.95	30	8	13
Cu_2O-derived Cu	0.5M $NaHCO_3$	-0.85	0.9	5.7	14
Pulsed-Cu (100)	0.1M $KHCO_3$	-1.0	-	5.5	15
Cu-P	0.1M $KHCO_3$	-1.15	9	5.1	16
Cu_8-3	1 M KOH	-1.3	216.3	~6	17
a-Zr/Cu	1M KOH	-0.8	70	14.4	18

Reference

1. J. Liu, P. Li, S. Jia, Y. Wang, L. Jing, Z. Liu, J. Zhang, Q. Qian, X. Kang, X. Sun, Q. Zhu，B. Han, *Nat. Synth.* 2025,**4**,730-743.
2. C. Peng, G. Luo, J. Zhang, M. Chen, Z. Wang, T.-K. Sham, L. Zhang, Y. Li，G. Zheng, *Nat. Commun.* 2021,**12**,1580.
3. K. Qi, Y. Zhang, N. Onofrio, E. Petit, X. Cui, J. Ma, J. Fan, H. Wu, W. Wang, J. Li, J. Liu, Y. Zhang, Y. Wang, G. Jia, J. Wu, L. Lajaunie, C. Salameh，D. Voiry, *Nat. Catal.* 2023,**6**,319-331.
4. B. Yang, L. Chen, S. Xue, H. Sun, K. Feng, Y. Chen, X. Zhang, L. Xiao, Y. Qin, J. Zhong, Z. Deng, Y. Jiao，Y. Peng, *Nat. Commun.* 2022,**13**,5122.
5. P. Grosse, D. Gao, F. Scholten, I. Sinev, H. Mistry and B. Roldan Cuenya, *Angew. Chem. Int. Ed.*, 2018, **57**, 6192-6197.
6. S. A. Francis, J. M. Velazquez, I. M. Ferrer, D. A. Torelli, D. Guevarra, M. T. McDowell, K. Sun, X. Zhou, F. H. Saadi, J. John, M. H. Richter, F. P. Hyler, K. M. Papadantonakis, B. S. Brunschwig and N. S. Lewis, *Chem. Mater.*, 2018, **30**, 4902-4908.
7. C. G. Morales-Guio, E. R. Cave, S. A. Nitopi, J. T. Feaster, L. Wang, K. P. Kuhl, A. Jackson, N. C. Johnson, D. N. Abram, T. Hatsukade, C. Hahn and T. F. Jaramillo, *Nat. Catal.*, 2018, **1**, 764-771.
8. Z. Han, R. Kortlever, H.-Y. Chen, J. C. Peters and T. Agapie, *ACS Cent. Sci.*, 2017, **3**, 853-859.
9. A. Loiudice, P. Lobaccaro, E. A. Kamali, T. Thao, B. H. Huang, J. W. Ager and R. Buonsanti, *Angew. Chem. Int. Ed*., 2016, **55**, 5789-5792.
10. N. S. Romero Cuellar, K. Wiesner-Fleischer, M. Fleischer, A. Rucki and O. Hinrichsen, *Electrochim. Acta*, 2019, **307**, 164-175.
11. S. Jeong, C. Huang, Z. Levell, R. X. Skalla, W. Hong, N. J. Escorcia, Y. Losovyj, B. Zhu, A. N. Butrum-Griffith, Y. Liu, C. W. Li, D. Reifsnyder Hickey, Y. Liu and X. Ye, *J. Am. Chem. Soc*., 2024, **146**, 4508-4520.
12. R. Zhang, J. Zhang, S. Wang, Z. Tan, Y. Yang, Y. Song, M. Li, Y. Zhao, H. Wang, B. Han and R. Duan, *Angew. Chem. Int. Ed.*, 2024, **63**, e202405733.
13. T.-T. Zhuang, Z.-Q. Liang, A. Seifitokaldani, Y. Li, P. De Luna, T. Burdyny, F. Che, F. Meng, Y. Min, R. Quintero-Bermudez, C. T. Dinh, Y. Pang, M. Zhong, B. Zhang, J. Li, P.-N. Chen, X.-L. Zheng, H. Liang, W.-N. Ge, B.-J. Ye, D. Sinton, S.-H. Yu and E. H. Sargent, *Nat. Catal.*, 2018, **1**, 421-428.
14. C. W. Li and M. W. Kanan, *J. Am. Chem. Soc*., 2012, **134**, 7231-7234.
15. R. M. Arán-Ais, F. Scholten, S. Kunze, R. Rizo and B. Roldan Cuenya, *Nat. Energy*, 2020, **5**, 317-325.
16. H. Li, X. Qin, T. Jiang, X. Y. Ma, K. Jiang and W. B. Cai, *ChemCatChem*, 2019, **11**, 6139-6146.
17. W. Dai, T. Qiao, K. Zhou, L. Peng, Y. Peng, J. Kuang, X. Yang, L. Cui, B. Wu, T. Xue, W. Hao, Y. Guo, H. Zhu, P. Su, S. Yang and J. Li, *Appl. Catal.*, B, 2026, **384**, 126154.
18. L. Zhou, Z. Huang, C. Guan, Y. Zhang, S. Bai, M. Kuang and J. Yang, *Adv. Funct. Mater.*, 2024, **35**, 2418727.